JOURNAL OF PROPULSION AND POWER
Vol. 24, No. 2, March–April 2008

Multicyclic-Detonation-Initiation Studies in Valveless Pulsed Detonation Combustors

Masayoshi Shimo* and Stephen D. Heister†
Purdue University, West Lafayette, Indiana 47907

DOI: 10.2514/1.29546

A pulsed detonation combustor was developed with the total absence of mechanical valves. The device was operated over a range of conditions with air and gaseous fuels (ethylene and propane) with both fuel streams and airstreams operating in valveless mode. This configuration allows a simplified design that could be used for propulsion and power generation systems as well as combined-cycle propulsion concepts. High-frequency pressure instrumentation reveals that overdriven detonations and Chapman–Jouguet detonations are generated within the device using both fuels. A novel vortex-generator design is employed to promote the deflagration-to-detonation transition process in a cyclic fashion. Pressure instrumentation within inlet manifolds confirms the capabilities of the configuration to cease fuel and air flows over a portion of the cycle. The character of wave development in the device is discussed, and a performance map is included to denote the range of operation in valveless mode.

Nomenclature

A	=	area
$\hat{C}^-$	=	first reflected characteristic to reach the thrust surface
c	=	speed of sound
c_1	=	speed of sound of the reactants
d_c	=	critical tube diameter
FF	=	volumetric fill fraction
f_{sp}	=	spark frequency
$\dot{m}$	=	mass flow rate
$\dot{m}_{mix}$	=	combustion mixture mass flow rate
$\dot{m}_{react}$	=	reactant mass flow rate
J^+	=	Riemann invariant on a right-facing characteristic
l	=	distance from inlet port to a pressure transducer
P	=	static pressure
P_1	=	initial pressure of the reactants
R	=	perfect-gas constant
T	=	static temperature
t	=	time
t_{delay}	=	time at which the first pressure rise is detected at a manifold after a spark initiation
t_{peak}	=	time at which a pressure peak is detected at a manifold
t_{BD}	=	time at which a blowdown starts
$t_{\hat{C}^-}$	=	time at which the first reflected characteristic reaches the thrust surface
t_{close}	=	time at which a gas-dynamic valve starts to close
t_{DDT}	=	time at which the deflagration-to-detonation transition process is initiated
t_{open}	=	time at which a gas-dynamic valve starts to open
u	=	flow velocity
u_1	=	flow velocity of the reactants
u_{fill}	=	fill velocity
$\dot{V}$	=	volumetric flow rate
V_{pdc}	=	valveless pulsed-detonation-combustor volume
x	=	position coordinate
ΔP	=	pressure difference
λ	=	cell width
γ	=	ratio of specific heats
ρ	=	density
ρ_{mix}	=	combustible mixture density
τ	=	gas-dynamic-valve cycle time
τ_{BD}	=	blowdown duration
$\tau_{\hat{C}^-}$	=	time taken by the first reflected characteristic to reach the thrust surface since spark initiation
τ_{close}	=	gas-dynamic-valve closing duration
τ_{DDT}	=	duration for deflagration-to-detonation transition process
τ_{fill}	=	fill duration
τ_{open}	=	gas-dynamic-valve opening duration
τ_{purge}	=	purge duration

Subscripts

BD	=	blowdown
close	=	valve close
DDT	=	deflagration-to-detonation transition
fill	=	fill
mix	=	combustible mixture
open	=	valve open
pdc	=	pulsed detonation combustor
purge	=	purge
react	=	reactant
spike	=	peak pressure at the thrust surface
1	=	state during the filling process
2	=	Chapman–Jouguet detonation state
3	=	state behind the Taylor wave during the detonation process

Presented as Paper 4308 at the 42nd AIAA/ASME/SAE/ASEE Joint Propulsion Conference & Exhibit, Sacramento, CCA, 9–12 July 2006; received 2 January 2007; revision received 12 August 2007; accepted for publication 4 October 2007.

*Senior Research Scientist, School of Aeronautics and Astronautics, 315 North Grant Street. Member AIAA.

†Professor, School of Aeronautics and Astronautics, 315 North Grant Street. Member AIAA.

I. Introduction

DEVICES categorized as pressure-gain combustors have been designed to achieve a nearly constant-volume combustion process that provides superior thermodynamic performance compared with a constant-pressure combustion process. A pulsed detonation combustor (PDC) is one of the pressure-gain combustors that can realize similar thermodynamic performance to constant-volume combustion process via unsteady detonation initiation. In particular, the Chapman–Jouguet (C–J) detonation takes a path similar to a constant-volume combustion process, which provides potential for higher thermodynamic performance than current

constant-pressure combustion devices. The entropy rise associated with a detonation process has been shown to be lower than that of a deflagration process for a given initial static condition. Foa [1] pointed out this conclusion with combustion entropy production estimates based on polytropic line analysis and argued that detonation offers better thermodynamic efficiency as a nonsteady mode than as a steady mode of combustion. Unsteady combustion processes avoid the continuous high-temperature exposure that is characteristic of steady-flow devices, thereby simplifying cooling of the combustor. Wintenberger et al. [2,3] showed that unsteady detonation systems provide the most thermodynamic potential for improvement over steady deflagration cycles used in current airbreathing propulsion systems. A similar conclusion was argued in 1940 by Zel'dovich [4] from the point of its entropy production caused by a shock wave coupled with a reaction zone.

One of the key technical challenges in PDC development is to control feed timing of combustible mixtures via various mechanical valving schemes. One of the innovative valving schemes was developed by Schauer et al. [5] using an automobile dual-overhead-cam cylinder head controlled by an electric motor to drive its camshafts. This configuration has demonstrated robust cyclic PDC operation for a wide range of hydrocarbon fuels in various operating conditions (frequency, fill fraction, and equivalence ratio). Several other groups have constructed similar systems following Schauer's lead. Another innovative valving scheme was developed by Bussing et al. [6,7], who proposed a rotary-valved multiple-combustor pulse detonation engine. This configuration employs several detonation chambers coupled to an air inlet and fuel source using a rotary valve composed of a plate and seal system with several orifices that alternately align with and block tube entry stations. The rotary valves provide isolation of steady air and fuel systems from the unsteady process of detonation by filling some detonation chambers while initiating detonation. Brophy et al. [8] developed a valveless PDC configuration using a fuel–oxygen system to initiate detonations in the main chamber. The initiator was operated by fast-acting solenoid valves to control feed timing of combustible mixtures. These valving schemes have successfully demonstrated their latent potential for PDC applications, but there are several problems that need to be dealt with, such as robustness, mechanical and thermal fatigue, cost, and internal flow dynamics during the fill and purge processes.

A valveless, or "aerovalved," configuration has previously been considered as an alternative to mechanical valving schemes. The design of the inlet passages of valveless configuration is more involved than for mechanical valving configuration, but a significant advantage of valveless configurations is the complete absence of moving parts and the attendant risk of their failure. This feature offers a benefit for a large pressure-gain combustor such as PDC, in which mechanical valves experience more arduous operating environments for a long operation time. In addition, the simplicity of a valveless design may permit incorporation into combined-cycle systems using other propulsive cycles for different flight regimes. However, the backflow of products of combustion emerging from the reactants inlet ports is a potential disadvantage for valveless configurations and must be carefully taken into account during the design of such a system.

To date, the bulk of aerovalve combustion studies have focused on the subsonic combustion (i.e., pulse jet applications). Pulse jet engines operate using nonsteady deflagration processes that provide a relatively low pressure rise (typically 10 to 100% of inlet stagnation pressure). Research and development efforts on valveless pulse jets were conducted during the World War II postwar period in France [9]. This group developed and tested a valveless pulse jet with a tapered tailpipe to maximize thrust production.

There are a few recent studies reporting valveless PDC operation. Baklanov et al. [10] reported that they built a valveless PDC using a chamber with a variable cross-sectional area similar to the Lockwood–Hiller design of a pulse jet to salvage a part of loss caused by the backflow effect. A schematic of their valveless pulsed detonation combustor is shown in Fig. 1. The device consists of fuel and air manifolds (8 and 9), detonation tube with flame accelerator

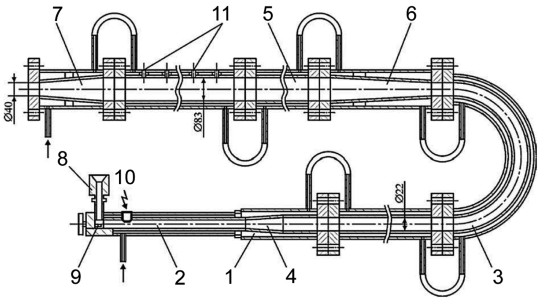

Fig. 1 Schematic of the Lockwood–Hiller type of valveless pulsed detonation device developed by Baklanov et al. [10].

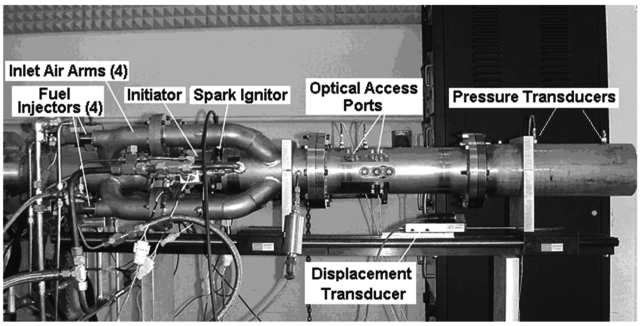

Fig. 2 Valveless pulsed detonation engine developed by Brophy et al. [11].

and several transition sections (2 to 7), water-cooling jacket (1), and a standard automobile spark plug (10). Vaporized gasoline and air are supplied separately through the manifolds in continuous fashion, leading to 2-Hz operation in valveless mode for durations as long as several hours. From the available literature, it is unclear whether the fuel was operated in a valveless configuration in this combustor.

Brophy and Hanson [11] designed a valveless configuration for their main chamber detonation initiation. Their valveless pulsed detonation combustor is shown in Fig. 2. The device is equipped with a main combustor connected with four fuel–air inlet arms and a fuel–oxygen-enriched air initiator to initiate detonations in the main combustor and operates on ethylene, propane, and JP-10. The initiator has a capability to operate at up to 100 Hz using high-speed solenoid valves, but the main combustor of this engine has only been evaluated at reduced-frequency operation ($\sim$40 Hz) in valveless mode, due to the detonation diffraction limits of the configuration. Initiation of the system via a spark igniter requires careful timing relative to the fuel valve initiation and aerovalve operation imposed by the particular flow resistance of the system. In general, this timing is determined empirically because the natural operating frequency in valveless-mode operation is not known a priori.

These devices have demonstrated some of the advantages of valveless PDC configuration, but there are several problems that need to be dealt with, such as compactness and requirements of easily detonable mixtures such as the ethylene–oxygen mixture for the initiator.

This paper describes the development and testing of an alternative configuration for valveless PDC applications. The present work differs from prior studies in that both the fuel and airstreams operate in valveless fashion in a linear configuration without the associated bend, as used in the Lockwood–Hiller concept outlined in Fig. 1. This configuration has the advantage of being rather compact relative to the Fig. 1 layout and is more amenable to aerospace propulsion applications in which the frontal area must generally be minimized to reduce vehicle drag. The following section highlights major design features of the device and the associated experimental facility. Operational conditions and test data are summarized in the subsequent sections of the paper, followed by conclusions from the studies.

II. Test Article and Facility Description

Experiments were conducted with a detonation combustor composed of three major components, as shown in Fig. 3. The detonation tube contains a Shchelkin spiral as a flame accelerator. The selection of blockage ratio, designed as the blocked area divided by the detonation tube cross-sectional area, was based on studies by Lindstedt and Michels [12], in which they quote 0.44 as the optimal blockage ratio for Shchelkin spiral configuration.

There are numerous reports regarding configurations of flame accelerators in connection with critical tube diameter [12–18], and the spiral configuration permits a smaller critical tube diameter than orifice-plate configurations. Lindstedt and Michels [12] argued that the use of orifice plates may be more closely associated with the behavior in the limit of detonation transmission through an abrupt area change providing $d_c \sim 13\lambda$ detonability limit criterion, where d_c and λ are the critical tube diameter and cell width, respectively. The spiral configuration can generate a single-head spinning detonation that produces a lower pressure loss when compared with an orifice-plate configuration.

The pitch size of the spiral is also a critical parameter to have successful deflagration-to-detonation transition (DDT) initiation of single-head spinning detonation (marginal detonation), and this was demonstrated in our previous studies using stoichiometric propane–air mixtures in a 76.2-mm detonation tube. One of the Shchelkin spirals tested in this experiment was fabricated from carbon steel rods with a blockage ratio of 0.43, a pitch size of 31.8 mm, and a length of 1 m, and it was not successful in initiating DDT for a large range of propane–air mixtures and fill conditions. An acceptable size of certain pitch size for single-head spin detonation is related to its spinning pitch size of the marginal detonation. Fay [19] and Moen et al. [20] found the detonability limit for spin pitch size based on the acoustic theories. Their theories predict the ratio of spin pitch to the critical tube diameter, and its pitch size was estimated on the order of the cell size for $d_c \sim \lambda/1.7$.

The vortex generator was constructed to provide sufficient flow recirculation zones for flame stabilization and mitigation of flame blowout under high-speed filling without a large pressure loss across a step. The vortex generator consisted of two different diameters of carbon steel tubes. As shown in Fig. 3, spark plugs and associated voltage discharge modules were used to ignite the combustible mixture upstream of the contracting section to create a quasi-stable recirculation zone of unsteady flow. There were multiple spark plugs mounted radially to assure ignition of the combustible mixture in this experiment. The total energy provided by the forced ignition is a miniscule amount compared with the critical energy required for direct initiation with stoichiometric ethylene–air (56 kJ) and stoichiometric propane–air combustible mixtures (215 kJ) [21].

The inlet face was installed at the middle of the vortex generator (downstream of the inlet section). The inlet face consisted of a stainless steel plate with an arrangement of desired porosity and shapes. The inlet face provides a key component for valveless operation and acts to serve as a fluid diode. A fluid diode emulates an aerodynamic check valve, providing the lowest possible resistance to inflow and the highest possible resistance to backflow [9]. The inlet face also serves as a mixing device during a filling process and a thrust surface during a backflow phase. The use of multiple holes promotes free shear flows within the vortex generator, thereby developing mixing layers that reduce mixing time and permit a higher operating frequency.

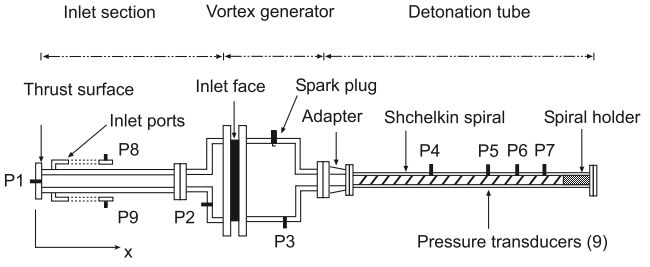

Fig. 3 Schematic of the valveless detonation test article configuration; P8 and P9 located at the manifolds.

The inlet section consisted of a carbon steel pipe and an instantaneous expanded section connected to the inlet face. The detailed schematic is described in Fig. 3. The longer inlet section effectively serves as a buffer zone to restrain backflow from reaching the inlet ports. A longer inlet provides a greater buffer zone at the expense of a longer flow time and reduced operating frequency. The instantaneous expanded section behind the inlet face also serves to enhance a preconditioning of a combustible mixture via a mixing process with the remaining combustion products from a previous cycle.

The ports for fuel and air supply were constructed of a 90-deg elbow and a solenoid valve for emergency shutoff. There are three inlet ports for the air supply and one for fuel supply, separately connected to the inlet section to impede flame propagation to manifolds during the backflow phase. A 180-deg return bend was used to provide the proper resistance and inertance within the respective flow paths. This device also serves as a thrust generator during the backflow phase to minimize backflow-induced pressure losses [9]. The number of inlet ports was estimated based on the desired range of valveless operating frequency and fill fractions. Air and fuel manifold pressures, which are estimated by their flow coefficients and expected mass flow rates in quasi-steady operation, set the aerodynamic valve operating times.

During operation in multicyclic mode, the entire valveless PDC was horizontally mounted on the test stand. The valveless PDC was filled in a cyclic fashion with ethylene–air or propane–air mixtures near stoichiometric conditions at various fill fractions and operating frequencies. Mass flow rates for fuel and air were controlled with sonic orifice plates placed well upstream of the test article. Averaged mass flow rates were controlled based on a volumetric fill fraction, an equivalence ratio, and an operating frequency of the valveless PDC. The sonic orifice plates were fabricated based on studies by Ward-Smith [22] showing that a square-edged orifice with a ratio of the orifice-plate thickness to bore diameter between 1 and 7 has a constant discharge coefficient to be 0.839. The operating frequency of the PDC was controlled by an ignition control system arranged with automobile ignition modules and digital timer/counter boards. The ignition control system is designed to provide digital pattern outputs to the ignition modules in 20-MHz external handshaking mode. The system can also accept 80-MHz digital output frequency to decide a certain event timing to control 32 ignition modules.

There were seven piezoelectric pressure transducers and two low-natural-frequency pressure transducers mounted in the locations indicated in Fig. 3: the thrust surface (P1), the inlet section (P2), the vortex generator (P3), fuel and air manifolds (P8 and P9), and along the detonation tube (P4-P7).

III. Flowfield Within the Valveless PDC

The wave propagation after a direct initiation of detonation is illustrated in the space–time wave diagram in Fig. 4, showing essential features of wave dynamics in an ideal situation. The analytical models of detailed wave propagation in the detonation tube have been proposed by Zel'dovich [4], and Taylor [23] proposed the propagation mechanism using the method of characteristics. A more elaborate analytical model of the detonation wave dynamics based on the method of characteristics was proposed by Wintenberger et al. [2] to estimate the impulse of single-cycle PDC. State 1 in Fig. 4 corresponds to the reactants filling the entire tube with velocity $u = u_{\text{fill}}$. State 2 represents the C–J state, followed by the self-similar expansion wave called the Taylor wave, just behind the detonation wave. The flow behind the C–J detonation wave (state 2) is subsonic relative to the tube for typical hydrocarbon fuel–air mixtures. The first reflected characteristic $\hat{C}^-$ emanates from the end of the tube when the detonation wave front reaches the interface between the combustion mixture and air at the open end of the tube. The slope of this $\hat{C}^-$ characteristic is specified by the interaction with the Taylor wave. The transmitted shock and contact surface propagate outside the detonation tube, and the flow expands

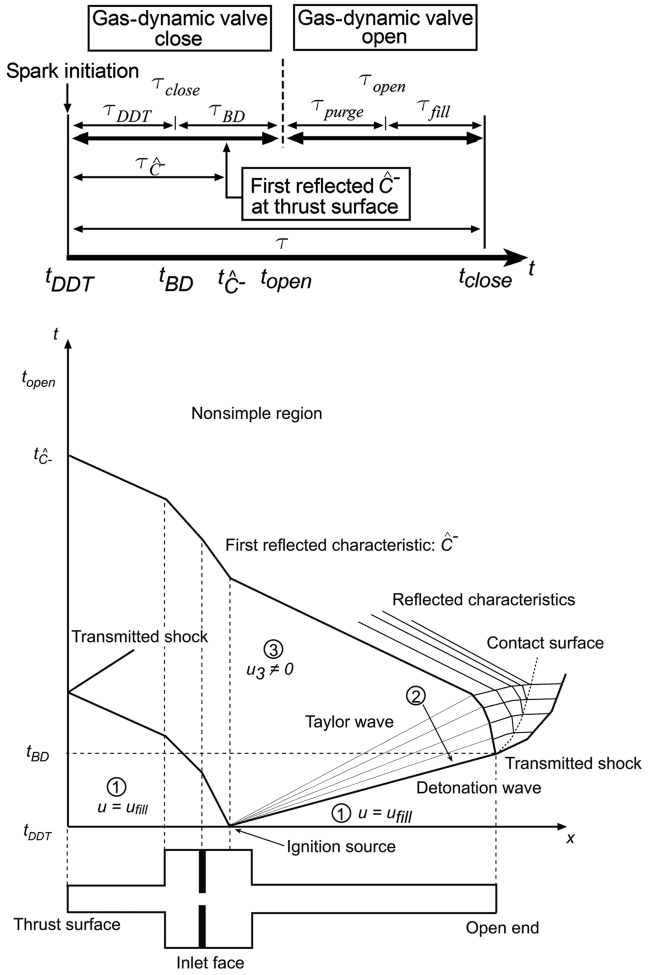

Fig. 4 Ideal space–time diagram for detonation wave and transmitted shock propagations inside of the valveless PDC with a timing diagram.

radially in three dimensions. The region behind the first reflected characteristic is a nonsimple region caused by interactions between the reflected expansion wave and the Taylor wave.

The Taylor wave causes the flow to expand, but because of the porous surface of the inlet face, the Taylor wave expands the flow from speed u_2 to a negative flow speed of u_3 in state 3 [24]. The first reflected characteristic $\hat{C}^-$ propagates at speed $[u_3 - c_3]u_3 + c_3$ after passing through the Taylor wave within state 3, where c is local speed of sound. This characteristic continues to propagate upstream through a variable cross-sectional area, reducing pressure at the thrust surface. The compression wave propagates toward the inlet section as a transmitted shock, due to the converging configuration of the vortex generator. The transmitted shock brings the reactant flow to rest at the inlet section and increases the pressure at the inlet section as a consequence of the backflow process. Fuel and airflows in the experiment are metered upstream such that the respective flow rates are insensitive to changes in manifold pressure; that is, upstream orifices remained choked throughout the process.

A gas-dynamic-valve cycle time of the valveless PDC is highly dependent on the detonation wave dynamics in the rig configuration. In general, a PDC cycle consists of four distinct processes occurring sequentially. The processes and associated time duration are defined as 1) detonation initiation and DDT process τ_{DDT}, 2) blowdown process τ_{BD}, 3) purge process τ_{purge}, and 4) fill process τ_{fill}, which are illustrated in detail in Fig. 4. The purging and filling processes occur when the gas-dynamic valve is open ($\tau_{open} = \tau_{purge} + \tau_{fill}$), whereas the gas-dynamic valve is closed during the DDT and blowdown processes ($\tau_{close} = \tau_{DDT} + \tau_{BD}$). Here, the end of the blowdown process is set by the time the gas-dynamic valve starts to open, due to depressurization of the inlet section caused by the reflected characteristics. The overall cycle time τ of the valveless PDC is obtained via summation of times associated with the four distinct processes:

$$\tau = \tau_{DDT} + \tau_{BD} + \tau_{purge} + \tau_{fill} = \tau_{close} + \tau_{open} \tag{1}$$

For successful operation, the spark interval time (which controls an operating frequency of the valveless PDC) must be greater than the overall cycle time τ. The gas-dynamic-valve opening duration τ_{open} consists of the purge and the fill processes. The time required for the fill process τ_{fill} can be approximately estimated assuming a one-dimensional uniform flow at ambient conditions entering the tube:

$$\tau_{fill} = \frac{\rho_{mix} V_{pdc}}{\dot{m}_{mix}} \tag{2}$$

where combustible mixture density ρ_{mix} and reactant mass flow rate $\dot{m}_{mix}$ are suitable average values for a given cycle. The combustible mixture density ρ_{mix} was approximated as an ambient condition, due to the low fill speed that is typical of operational conditions. The time required for the purge process τ_{purge} can be estimated by the interval between initiation of self-aspiration of air and initiation of self-aspiration of the fuel. In general, the purge time may be significantly lower than the fill time τ_{fill}. The purge process creates a small buffer zone between reactants and products to prevent autoignition of the reactants during the fill process. The timing and duration of the purge process are dependent on the configuration of the valveless PDC and respective manifold pressure.

The gas-dynamic-valve closing duration τ_{close} consists of the DDT process and the blowdown process. The gas-dynamic-valve closing duration is also related to the characteristic time $t_{\hat{C}^-}$, as depicted in Fig. 4. The pressure at the thrust surface remains constant until the first reflected characteristic from the tube's open end reaches the thrust surface at time $t_{\hat{C}^-}$ [2]. When the thrust surface and inlet section are pressurized, fuel and air mass fluxes from their inlet ports are decelerated by a compression wave by the following relation based on the method of characteristics:

$$\frac{u}{c_1} = \frac{J^+}{c_1} - \frac{2}{\gamma - 1}\left(\frac{P}{P_1}\right)^{\frac{\gamma-1}{2\gamma}} \left(< \frac{u_1}{c_1}\right) \tag{3}$$

assuming that a transmitted shock wave propagating to upstream of manifolds in Fig. 4 maintains isentropic condition. Here, J^+ and P represent a Riemann invariant on a right-facing characteristic and local pressure, respectively. If local pressure P is large enough compared with initial fill pressure P_1, the nondimensional local velocity described in Eq. (3) is reduced to terminate the filling process (i.e., the gas-dynamic valve is in a closed state). The gas-dynamic valve remains closed until the thrust surface is depressurized. When the inlet section is depressurized, an expansion wave is initiated and propagates into manifolds, causing acceleration of fuel and air masses. The gas-dynamic-valve closing duration is set by the size of the valveless PDC, including the manifold arrangement that regulates the arrival of reflected characteristics, and the minimum manifold pressure, which regulates onset of the closing and opening times of the gas-dynamic valve. A similar gas-dynamic-valve characteristic was discussed in pulse jet development in terms of manifold pressure and configuration (valve area ratio) [1,25,26], in which an increase of manifold pressure or valve area ratio leads pulse combustion mode to constant-pressure combustion mode (ramjet mode).

To estimate the gas-dynamic-valve closing duration τ_{close}, fuel and air manifold pressures were measured. The gas-dynamic-valve closing duration is estimated by measuring the time between spark initiation t_{DDT} and peak pressure detected at each manifold, t_{peak}:

$$\tau = \tau_{close} + \tau_{open} \approx (t_{peak} - t_{DDT}) + \tau_{fill} \tag{4}$$

assuming that $\tau_{purge} \ll \tau_{fill}$ and $t_{peak} \approx t_{open}$. The spark-initiation interval must be greater than the gas-dynamic cycle time τ, which controls an operating frequency of the valveless PDC.

Table 1 Experimental conditions of the valveless PDC operation

Reactant	Frequency, Hz	Fill fraction	ϕ
C_2H_4–air	5.3–8.3	1.1–2.0	0.7–1.1
C_3H_8–air	1.5–6.3	0.9–2.6	0.8–1.2

IV. Experimental Results

A. Pressure Data for the DDT Process

Experiments were conducted using ethylene and propane fuels combusted with air. The pressure data are presented in this section to illustrate the internal flowfield in the detonation tube. Although the rig was operated to reach thermal steady-state conditions, the duration of an operating sequence for data acquisition was reduced to less than 10 s to protect instrumentation. In total, approximately 50 tests were conducted with propane and ethylene fuels over the range of conditions shown in Table 1. All experiments were conducted with initial-atmospheric-pressure air occupying the combustor. Highlighted results from the study are presented in the remainder of this section.

To illustrate operation of the device in valveless detonating mode, ethylene–air cases at an averaged equivalence ratio of 1.1 and operating frequency of 5.26 Hz are presented. Typical time histories of multicyclic pressure pulses measured along the detonation tube are presented in Figs. 5a and 6a to show repeatability of combustion waves. Figures 5b and 6b represent a single-pulse history obtained from the multicyclic operation with a specified fill fraction. Figures 5b and 6b also show the C–J detonation pressures (1.89 MPa) and the pressures at state 3 behind the Taylor wave, assuming direct initiation at the closed end of the tube as a reference (0.75 MPa) [2]. There are variations of pressure magnitude for each wave, as shown in Figs. 5a and 6a, but Figs. 5b and 6b represent general trends for their specific conditions. To clarify a wave propagation process, the time axis is taken on the abscissa, in which zero corresponds to the reference pressure. Tracking each peak of a pressure history permits construction of the pressure wave trajectory down the tube and the DDT process. Data in Fig. 5b indicate flame acceleration to denotation by the time the wave reaches the location of transducer P5, with peak pressures in excess of 4 MPa at this location.

Data for fill fractions of approximately 1.7 and 1.1 appear in Figs. 5b and 6b, respectively. Note that the fill fractions were estimated by the following equation:

$$\mathrm{FF} = \frac{\dot{V}\{(1/f_{\mathrm{sp}}) - \tau_{\mathrm{close}}\}}{V_{\mathrm{pdc}}} \tag{5}$$

$$\approx \frac{\dot{V}\{(1/f_{\mathrm{sp}}) - (t_{\mathrm{peak}} - t_{\mathrm{DDT}})\}}{V_{\mathrm{pdc}}} \tag{6}$$

where f_{sp}, FF, t_{DDT}, t_{peak}, V_{pdc}, and $\dot{V}$ represent spark frequency, volumetric fill fraction, time at which DDT process is initiated, time

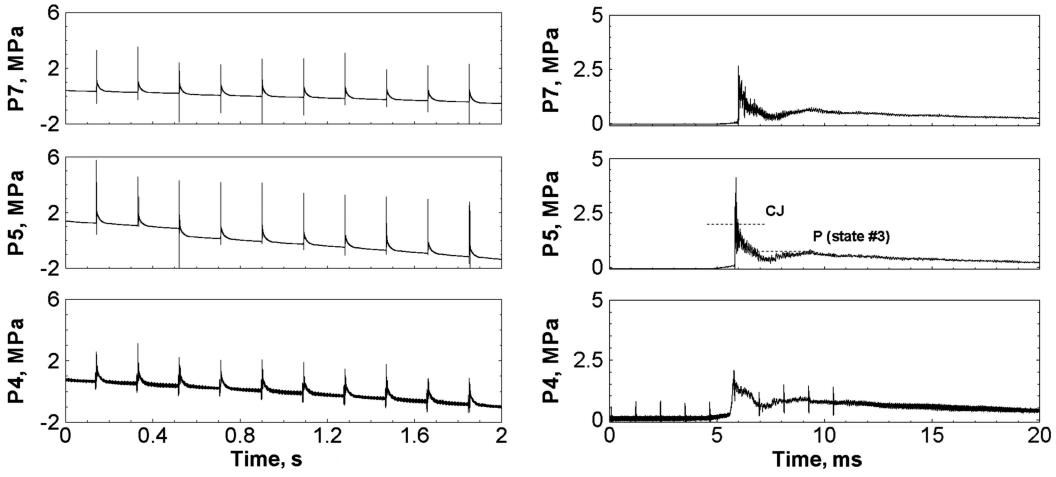

Fig. 5 Pressure histories recorded for C_2H_4–air mixture with a fill fraction of 1.7: a) multicyclic and b) single pulse.

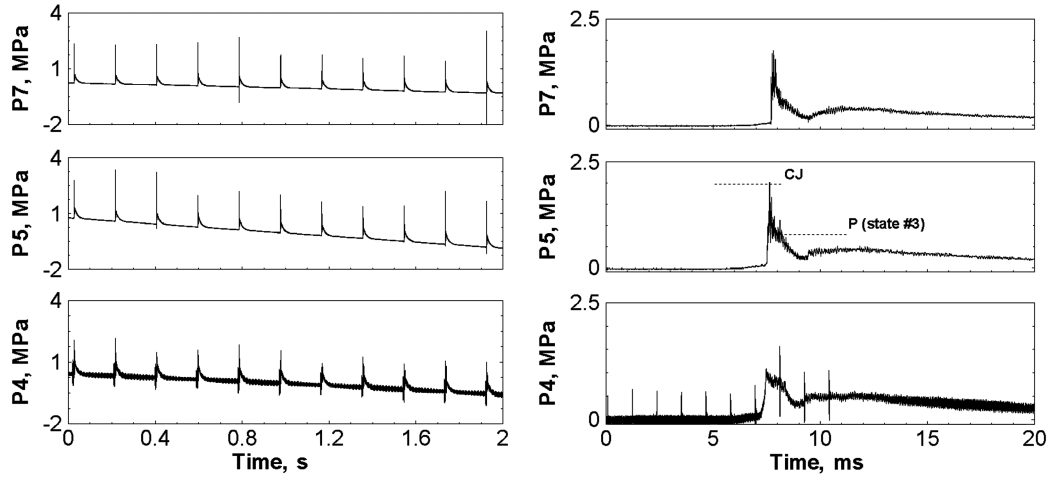

Fig. 6 Pressure histories recorded for C_2H_4–air mixture with a fill fraction of 1.1: a) multicyclic and b) single pulse.

Table 2 List of DDT initiation results

Reactant	Fill fraction	ϕ	Flame type
C_2H_4–air	0.7	0.9	Quasi-detonation regime
C_2H_4–air	0.7	1.0	Quasi-detonation regime
C_2H_4–air	0.8	1.0	Quasi-detonation regime
C_2H_4–air	1.0	1.0	Quasi-detonation regime
C_2H_4–air	1.1	1.1	Choked-flame regime
C_2H_4–air	1.7	1.1	Detonation
C_3H_8–air	2.3	1.0	Choked-flame regime
C_3H_8–air	2.3	1.1	Detonation
C_3H_8–air	2.3	1.2	Detonation

at which a pressure peak is detected at a manifold, valveless PDC volume, and volumetric flow rate, respectively. The large fill fractions required to attain maximum performance are indicative of poor mixing of the fuel streams and airstreams. A partial list of the DDT initiation results with ethylene–air and propane–air mixtures are presented in Table 2 to clarify the poor mixing performance of the test rig. During the evaluations, three separate regimes were encountered: 1) detonation, 2) quasi-detonation regime, and 3) choked regime based on their wave speeds. Lower-fill-fraction cases generally provide quasi-detonation regimes in which wave speeds typically reside between the C–J detonation and the choked-flame speeds. The detonation wave propagation can be easily disturbed by internal configurations and local equivalence ratio. Recent investigations [11,27] have also indicated that mixture ratio striations are prevalent in many practical partial-differential-equation configurations, and successful operation is attained when near-stoichiometric mixtures are produced at the proper time near the igniter location. The injection configuration, fluid types, transient operating conditions, and local turbulence levels can all contribute to the detailed mixing and transport within the combustor. Design of the valveless configurations must be conducted properly to ascertain a proper mixing distribution in multicyclic operation. However, optimization of the mixing process was not the objective of the present study and it would clearly need to be improved for operation within a practical device. In addition, a high fill fraction implies higher overall flow rate and higher pressure in the combustor for DDT initiation. Practical devices could raise pressures at initiation via the use of a throat/nozzle in the combustor exit region.

At a 1.7 fill fraction (Fig. 5b), the maximum peak pressure is 4.18 MPa, which is greater than the Chapman–Jouguet detonation pressure of 1.89 MPa, indicating potential presence of an overdriven detonation. The wave speed is 1917 m/s measured between P5 and P7, which is greater than the Chapman–Jouguet detonation speed of 1846 m/s. At a 1.1 fill fraction (Fig. 6b), the maximum peak pressure is 2.04 MPa, which is close to the Chapman–Jouguet detonation pressure of 1.89 MPa, but the wave speed is 1104 m/s measured between P5 and P7, indicating that it resides in a choked-flame regime or that a pressure wave decoupled from a reaction zone. Nevertheless, the aerovalve appears to function within this subdetonative regime.

Pressure data for a propane–air combustion mixture with an average $\phi = 1.1$ and an operating frequency of 1.54 Hz are presented in Fig. 7. Figure 7 also shows the C–J detonation pressures (1.88 MPa) and the pressures at state 3 behind the Taylor wave, assuming direct initiation at the closed end of the tube as a reference (0.74 MPa) [2]. At a 2.3 fill-fraction condition, the maximum peak pressure is 4.93 MPa and the wave speed is 2116 m/s, which are greater than the C–J values of 1.88 MPa and 1819 m/s, respectively.

Although the equivalence ratios of these fill-fraction conditions are the same, different combustion behavior was observed in the detonation tube. This observation is associated with the fact that an actual filling time is regulated by the filling/mixing process in a certain configuration of PDC. In the time required to get a sufficient fill of PDC for DDT, initiation is reduced by a higher-set fill fraction (i.e., mass flow rate) and a lower-set fill fraction may not provide enough combustible mixture within a spark interval time to initiate a DDT. Note that a higher fill fraction increases fill speed but simultaneously causes flame stabilization problems in this head-end filling configuration. We next discuss the impacts of fill fraction on attributes of the valveless PDC in more detail, and its cycle time is discussed in a later section.

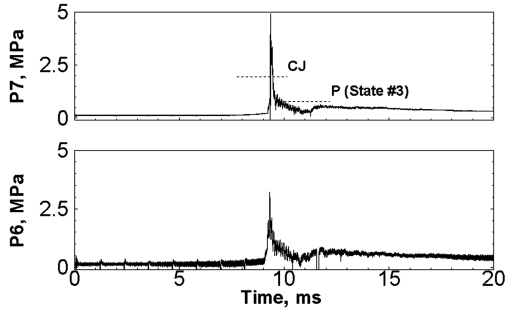

Fig. 7 Single-pulse pressure histories recorded for C_3H_8–air mixture.

B. Pressure Data at the Inlet Section and the Vortex Generator

The pressure data at the inlet and vortex-generator sections appear in Fig. 8 for an ethylene–air mixture with an equivalence ratio of 1.1 and operating frequency of 5.26 Hz, but different fill fractions of 1.7 and 1.1. The ignition sources were located at the vortex-generator section (Fig. 3) so that the first pressure rise was detected by the pressure transducer P3. A transmitted compression wave propagating toward the thrust surface is observed in the pressure histories, as described in Fig. 4.

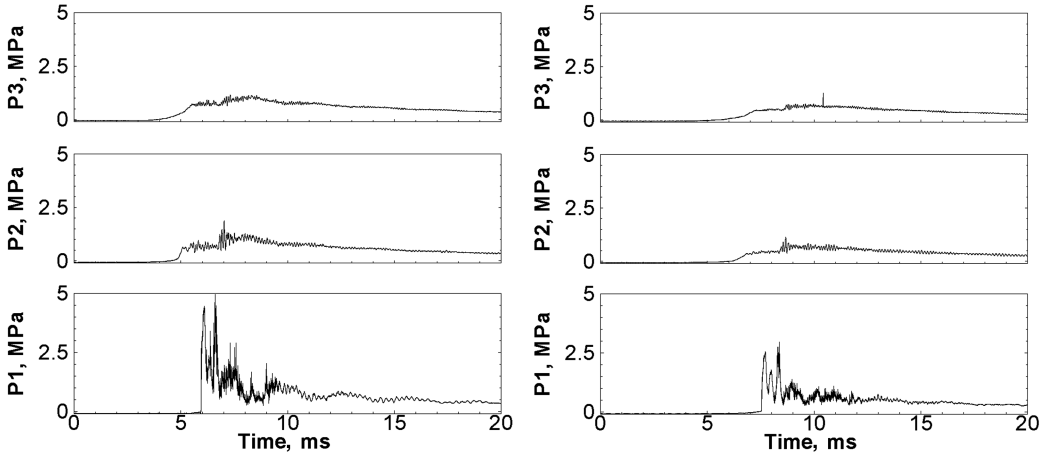

Fig. 8 Pressure histories recorded at the inlet and vortex-generator sections for C_2H_4–air mixture with a fill fraction of a) 1.7 and b) 1.1.

Table 3 Comparisons between pressure at the thrust surface for a straight tube configuration estimated by Wintenberger [28] and pressure measured at the trust surface in the valveless PDC

Data source	ϕ	Fill fraction	P_1, MPa	T_1, K	P_{spike}, MPa	P_3, MPa	t_{spike}, ms
Wintenberger [28]	1.0	1.0	0.1	300	1.825	0.684	-
Present work	1.1	1.7	0.1	298	>4.46	>0.67	>0.5
Present work	1.1	1.1	0.1	298	>2.56	>0.34	>0.5

A significant pressure rise is detected at the thrust surface (P1) for the fill fraction of 1.7, as shown in Fig. 8a, due to a transmitted shock propagation on area convergence that is stronger than the incident shock [28]. There are two peak pressure spikes over 4 MPa detected at P1 within 1 ms. These values exceed the C–J detonation pressure of 1.89 MPa. A plateau pressure region including these two pressure spikes appears for about 7 ms (6–13 ms) at P1, which is followed by a region of decreasing pressure caused by numerous reflected characteristics within the blowdown process. The other plateau regions detected at P2 and P3 also appear for about 7 ms (5–12 ms for both P2 and P3), followed by a blowdown process. A reflected shock at the thrust surface is observed as a weak pressure spike at the pressure transducers located at P2 and P3 around 7 ms in Fig. 8a. The onset of pressure decrease due to arrival of the first reflected characteristic $\hat{C}^-$ is observed at the P3 transducer close to the exit end of detonation tube.

A similar pressure–time behavior is also measured at the thrust surface (P1) for the fill fraction of 1.1, as shown in Fig. 8b. However, the strength of the transmitted shock is much smaller than for the fill fraction of 1.7, indicating a failure to initiate successful DDT, as shown in Fig. 6. There are two peak pressure spikes over 2 MPa detected at P1 within 1 ms (Fig. 8b). A plateau pressure region including these two pressure spikes appears for about 6 ms (7–13 ms) at P1, which is followed by a region of decreasing pressure caused by numerous reflected characteristics, as shown in Fig. 8b. The other plateau regions detected at P2 and P3 also appear for about 6 ms (7–13 ms for both P2 and P3), which are also followed by a region of decreasing pressure caused by numerous reflected characteristics, as shown in Fig. 8b. A reflected shock at the thrust surface is observed as a weak pressure spike at the pressure transducers located at P2 and P3 around 9 ms in Fig. 8b.

The pressure–time traces detected at P1 for both the 1.7 and 1.1 fill fractions were compared with the idealized pressure–time trace model at the thrust surface for a straight detonation tube proposed by Wintenberger et al. [2], which are given in Table 3. A schematic of the idealized pressure–time trace is presented in Fig. 9. Both of the pressure peaks measured at the thrust surface are higher than the value associated with the C–J detonation for a straight detonation tube, partly due to the contracting configuration of the inlet section. Successful DDT initiation for the fill fraction of 1.7 creates higher-magnitude pressure waves than for the fill fraction of 1.1, which is likely attributed to the higher combustor flow rates at the higher-fill-fraction condition. In addition, there is ignition delay observed in Fig. 8b compared with Fig. 8a, which may be attributed to multidimensional effects and the larger velocities associated with the higher-fill-ratio condition. Note that the gas-dynamic valve functioned for both fill fractions of 1.1 and 1.7, as long as the magnitude of the transmitted shock has a certain value associated with manifold pressure, as discussed in the following section.

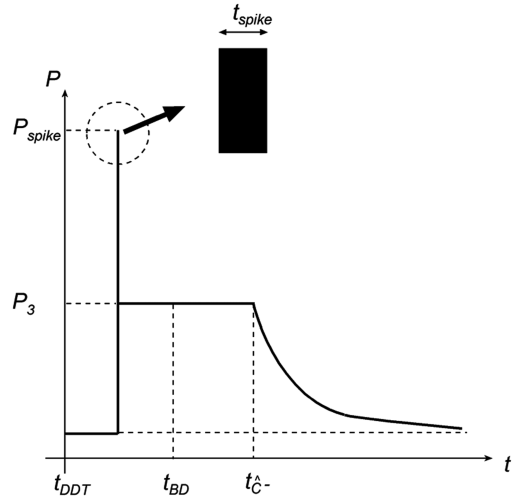

Fig. 9 Idealized model of pressure history at the thrust surface [2].

C. Manifold Pressure Measurements

Typical pressure data for the fuel and air manifolds (P8 and P9 in Fig. 3) are depicted in Figs. 10 and 11 for the case of an ethylene–air mixture with an equivalence ratio of 1.1 and operating frequency of 5.26 Hz at fill fractions of 1.7 and 1.1, respectively. The time of spark initiation corresponds to $t = 0$ ms in these figures. A pressure rise caused by a pressure buildup at the inlet section is observed in both fuel and air manifold in Figs. 10 and 11. There are pressure oscillations detected in the fuel manifold (P8) pressure rise for both the fill fractions, due to longitudinal mode of acoustic oscillations in the inlet section. Similar oscillation is also detected for the air

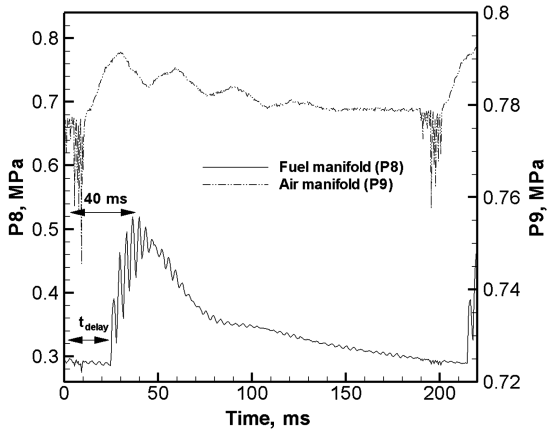

Fig. 10 Pressure histories at fuel and air manifold recorded for C_2H_4–air mixture with a fill fraction of 1.7.

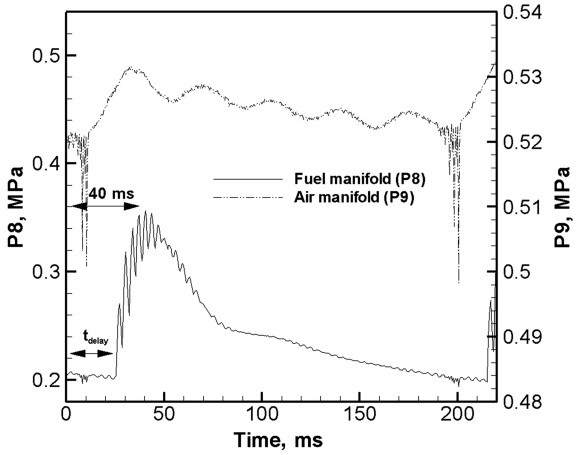

Fig. 11 Pressure histories at fuel and air manifold recorded for C_2H_4–air mixture with a fill fraction of 1.1.

manifold's pressure history (P9) with much lower frequency. The oscillation frequencies for the fuel side are in the 300–330-Hz range for both fill fractions, whereas oscillation frequencies for the air side are in the 25–35-Hz range for the two cases.

As shown in Fig. 4, the transmitted shock reflected at the thrust surface continues to reflect in the inlet section between the inlet face and the thrust surface, causing the longitudinal mode of acoustic oscillations. The pressure oscillations caused by the transmitted shock reflections are also observed at the thrust surface (P1) pressure histories, as shown in Fig. 8. The acoustic oscillation frequencies of the fuel side detected at P8 are always higher amplitude than the air side (location P9), due to the relatively larger inertia of the airstream. Fuel-side pressure oscillations are acoustic in nature, whereas the lower frequency air-side oscillations correlate more closely with a bulk mode involving the fluid in the line downstream of the orifice plate. The pressure difference at the inlet port allows a transmitted compression wave to propagate toward both fuel and air manifolds, resulting in deceleration of the entire reactant flow flux. The gas-dynamic valve is effectively closed until the respective manifold pressures start to decrease. The set pressures are controlled such that the air begins to flow before the fuel, thereby insuring some purge gas between successive pulses.

Figure 10 shows that minimum manifold pressures for the air and fuel systems are approximately 0.78 and 0.29 MPa, respectively. A combination of fuel and air minimum manifold pressures regulates timing of purging and filling processes in the valveless PDC. Because the manifold pressure for the air is higher than that of the fuel, the gas-dynamic valve for the air opens before the fuel, thereby providing a mechanism to initiate a purging of combustion products before initiation of the subsequent cycle. The purging process creates a buffer zone between combustion products and newly charged reactants, which prevents preignition of the fresh reactants. Fuel is not supplied until pressure at the inlet section is low enough to generate an expansion wave transmitted to the fuel manifold having adequate pressure drop across the manifold.

Using the method of characteristics, the time required for the head of a compression wave to reach the manifold can be computed. Assuming that mass flow in a reactant supply line is subsonic, the speed of the first characteristic propagating upstream to the manifold is

$$C^-: \frac{\mathrm{d}x}{\mathrm{d}t} = u - c = \frac{\dot{m}}{\rho A} - \sqrt{\gamma RT} \tag{7}$$

where $\dot{m}$, ρ, A, γ, R, and T represent mass flow rate, density, cross-sectional area of supply line, specific heat ratio, and static temperature, respectively. Note that the left-facing characteristic described in Eq. (7) propagates through the inlet ports toward pressure transducers (P8 and P9) at the manifolds described in Fig. 3. The time when the pressure transducer at the manifold detects the head of compression wave can be computed as

$$t_{\mathrm{delay}} = \frac{l}{|u - c|} = \frac{l}{|(\dot{m}/\rho A) - \sqrt{\gamma RT}|} \tag{8}$$

where l represents distance from an inlet port to a pressure transducer. The pressure transducers at the fuel manifold (P8) and at the air manifold (P9) detected their pressure rises at 11 ms (estimated time of 13.0 ms) and 25 ms (estimated time of 28.9 ms), as shown in Fig. 10, having a reasonable agreement with estimated times. Pressure peaks detected at the air and fuel manifolds appear approximately 30 and 40 ms, respectively, from spark initiation, which are relatively consistent in every cycle and for both fill fractions (Figs. 10 and 11). The gas-dynamic valves for the air and fuel lines start to open after passing these peaks. The magnitude of the pressure peak is lower for the lower-fill-fraction condition, due to the lower flow rate implied by this condition.

D. Spark Frequency Versus Cycle Frequency

The performance of the device was assessed over a wide range of spark intervals. Figure 12 illustrates the effect of the gas-dynamic-valve cycle time on spark interval, which controls operating frequency of the valveless PDC. The cycle time is approximately estimated using Eq. (4), assuming that the τ_{purge} is negligible compared with τ_{fill}, and τ_{close} is approximated to be a duration between the time of the spark initiation and of the peak pressure detected at the fuel manifold, $t_{\mathrm{peak}} - t_{\mathrm{DDT}}$. The fill duration τ_{fill} is estimated by Eq. (2). Reference for the cycle time corresponds to the spark initiation t_{DDT}. This plot includes all data points describing pulsed combustion modes, regardless of their DDT accomplishments. Successful mode designates that a spark frequency corresponds with an actual operating frequency. The gas-dynamic-valve cycle time is required to be less than the spark interval to synchronize spark-initiation frequency. Reduction of fill time can be achieved by increasing a fill fraction, reducing a combustor size, or optimizing a filling scheme.

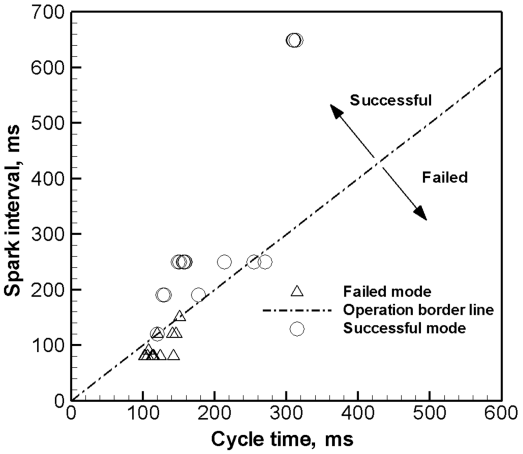

Fig. 12 Relation between the spark interval and the gas-dynamic-valve cycle time to describe a possible operational region with the valveless PDC.

V. Conclusions

A valveless pulsed detonation combustor was developed and multicyclic operation was demonstrated using ethylene–air and propane–air mixtures. The configuration offers an advantage with respect to its complete absence of moving parts, which permits the development of minimum complexity in pulsed detonation combustors. The device has produced overdriven detonation conditions within the detonation tube with both ethylene and propane fuels. The combustor consisted of three components: the inlet section, the vortex generator, and the detonation tube. The inlet section consists of a buffer zone and an inlet face composing a fluid diode that provides a maximum resistance during a backflow process and provides a minimum resistance during an inflow process. The inlet face is a critical component of the valveless PDC, which contributes as a thrust surface, a fluid diode, and a mixing device. The vortex generator functions as a flame stabilization and a mixing device.

Experiments were completed with near stoichiometric ethylene–air and propane–air mixtures and various fill fractions at standard atmospheric conditions. Pressure measurements in the inlet section and vortex generator indicate that a transmitted shock propagates to the inlet section during a backflow phase, preventing reactant inflow from entering the vortex-generator section. After the transmitted shock wave is reflected at the thrust surface, the entire inlet section was found to be pressurized, to allow a gas-dynamic valve to close until reflected characteristics at the end of detonation tube reach the inlet section. The gas-dynamic valve was found to be able to function regardless of the combustion mode in the detonation tube.

Acknowledgments

This work was supported by a grant from the Indiana 21st Century Research and Technology Fund and Rolls-Royce North America.

We are grateful to Lynn Snyder at Rolls-Royce North American Technologies, Inc., for his continuous support. We also thank senior engineer Scott Meyer and technician Rob McGuire for their helpful suggestions and assistance with the design, fabrication, and testing of the test articles.

References

[1] Foa, J. V., *Elements of Flight Propulsion*, Wiley, New York, 1960.

[2] Winterberger, E., Austin, J. M., Cooper, M., Jackson, S., and Shepherd, J. E., "Analytical Model for the Impulse of Single-Cycle Pulse Detonation Tube," *Journal of Propulsion and Power*, Vol. 19, No. 1, 2003, pp. 22–38.

[3] Winterberger, E., and Shepherd, J. E., "Stagnation Hugoniot Analysis for Steady Combustion Waves in Propulsion Systems," *Journal of Propulsion and Power*, Vol. 22, No. 4, 2006, pp. 835–844.

[4] Zel'dovich, Y. B., "On the Use of Detonative Combustion in Power Engineering," *Journal of Technical Physics*, Vol. 10, No. 17, 1940, pp. 1453–1461.

[5] Schauer, F., Stutrud, J., and Bradley, R., "Detonation Initiation Studies and Performance Results for Pulsed Detonation Engines," AIAA Paper 2001-1129, Jan. 2001.

[6] Bussing, T. R. A., "A Rotary Valved Multiple Pulse Detonation Engine," AIAA Paper 1995-2577, 10–12 July 1995.

[7] Hinkey, J. B., Henderson, S. E., and Bussing, T. R. A., "Operation of a Flight-Scale Rotary-Valved, Multiple-Combustor, Pulse Detonation Engine (RVMPDE)," AIAA Paper 1998-3881, 13–15 July 1998.

[8] Brophy, C. M., Sinibaldi, J. O., and Damphousse, P., "Initiator Performance for Liquid-Fueled Pulse Detonation Engines," AIAA Paper 2002-0472, 2002.

[9] Kentfield, J. A. C., *Nonsteady, One-Dimensional, Internal, Compressible Flows Theory and Applications*, Oxford Univ. Press, Oxford, 1993.

[10] Baklanov, D. I., Gvozdeva, L. G., and Scherbak, N. B., "Investigation of Pulse-Detonation Engine Operating on Gasoline–Air Mixture," *Proceedings of the 14th ONR Propulsion Meeting*, Office of Naval Research, Arlington, VA, 2001, pp. 148–153.

[11] Brophy, C. M., and Hanson, R. K., "Fuel Distribution Effects on Pulse Detonation Engine Operation and Performance," *Journal of Propulsion and Power*, Vol. 22, No. 6, 2006, pp. 1155–1161. doi:10.2514/1.18713

[12] Lindstedt, R. P., and Michels, H. J., "Deflagration to Detonation Transitions and Strong Deflagrations in Alkane and Alkene Air Mixtures," *Combustion and Flame*, Vol. 76, No. 2, May 1989, pp. 169–181. doi:10.1016/0010-2180(89)90065-5

[13] Cooper, M., Jackson, S., Austin, J., Wintenberger, E., and Shepherd, J. E., "Direct Experimental Impulse Measurements for Detonations and Deflagrations," *Journal of Propulsion and Power*, Vol. 18, No. 5, 2002, pp. 1033–1041.

[14] Lee, J. H. S., "Detonation Waves in Gaseous Explosives," *Handbook of Shock Waves*, edited by G. Ben-Dor, O. Igra, T. Elperin, and A. Lifshitz, Vol. 3, Academic Press, London, 2001, pp. 309–415.

[15] Manzhalei, V. I., "Low-Velocity Detonation Limits of Gaseous Mixtures," *Combustion, Explosion, and Shock Waves*, Vol. 35, No. 3, May 1999, pp. 296–302. doi:10.1007/BF02674453

[16] Peraldi, O., Knystautas, R., and Lee, J. H., "Criteria for Transition to Detonation in Tubes," *Proceedings of the 21st Symposium on Combustion*, Combustion Inst., Pittsburgh, PA, 1986, pp. 1629–1637.

[17] Wolanski, P., Kauffman, C. W., Sichel, M., and Nicholls, J. A., "Detonation of Methane–Air Mixtures," *Proceedings of the 18th Symposium on Combustion*, Combustion Inst., Pittsburgh, PA, 1981, pp. 1651–1660.

[18] Zel'dovich, Y., Kogarko, S., and Simonov, N., "An Experimental Investigation of Spherical Detonation," *Soviet Physics Technical Physics*, Vol. 1, No. 8, 1956, pp. 1689–1713.

[19] Fay, J. A., "A Mechanical Theory of Spinning Detonation," *The Journal of Chemical Physics*, Vol. 20, No. 6, 1952, pp. 942–950. doi:10.1063/1.1700655

[20] Moen, I. O., Donato, M., Knystautas, R., and Lee, J. H., "The Influence of Confinement on the Propagation of Detonations Near the Detonability Limits," *Proceedings of the 18th Symposium on Combustion*, Combustion Inst., Pittsburgh, 1981, pp. 1615–1623.

[21] Kaneshige, M., and Shepherd, J. E., "Detonation Database," Explosion Dynamics Lab., Graduate Aeronautical Labs., California Inst. of Technology, Rept. FM97-8, Pasadena, CA, 1999.

[22] Ward-Smith, A. J., "Critical Flowmetering: The Characteristics of Cylindrical Nozzles with Sharp Upstream Edges," *International Journal of Heat and Fluid Flow*, Vol. 1, No. 3, 1979, pp. 123–132. doi:10.1016/0142-727X(79)90028-6

[23] Taylor, G. I., "The Dynamics of the Combustion Products Behind Plane and Spherical Detonation Fronts in Explosives," *Proceedings of the Royal Society, A*, Vol. 200, The Royal Society, London, 1950, pp. 235–247.

[24] Cooper, M., and Shepherd, J. E., "Effect of Porous Thrust Surfaces on Detonation Transition and Detonation Tube Impulse," *Journal of Propulsion and Power*, Vol. 20, No. 5, 2004, pp. 811–819.

[25] Foa, J. V., "Intermittent Jets," *Jet Propulsion Engines*, Vol. 12, Princeton Univ. Press, Princeton, NJ, 1959, pp. 377–438.

[26] Schultz-Grunow, F., "Gas-Dynamic Investigation of the Pulse-Jet Tube," NACA TM-1131, 1947.

[27] Ji, J., Shimo, M., Heister, S., and Gore, J., "Combustion Diagnostics of the Cyclic Pulse Detonation Process with Infrared Spectroscopy," AIAA Paper 2003-4823, July 2003.

[28] Wintenberger, E., "Application of Steady and Unsteady Detonation Waves to Propulsion," Ph.D. Dissertation, Graduate Aeronautical Labs., California Inst. of Technology, Pasadena, CA, 2004.

[29] Oppenheim, A. K., Urtiew, P. A., and Stern, R. A., "Peculiarity of Shock Impingement on Area Convergence," *The Physics of Fluids*, Vol. 2, No. 4, 1959, pp. 427–431. doi:10.1063/1.1724414

J. Powers
Associate Editor